Structural Characterization and Catalytic Activity of Nanosized Ceria–Terbia Solid Solutions

ARTICLE *in* THE JOURNAL OF PHYSICAL CHEMISTRY C · SEPTEMBER 2008

Impact Factor: 4.77 · DOI: 10.1021/jp806131r

Structural Characterization and Catalytic Activity of Nanosized Ceria−Terbia Solid Solutions

Benjaram M. Reddy,*,† Pranjal Saikia,† Pankaj Bharali,† Yusuke Yamada,‡ Tetsuhiko Kobayashi,‡ Martin Muhler,§ and Wolfgang Grünert§

Inorganic and Physical Chemistry Division, Indian Institute of Chemical Technology, Hyderabad 500 607, India, National Institute of Advanced Industrial Science and Technology, 1-8-31 Midorigaoka, Ikeda, Osaka, 563-8577, Japan, Lehrstuhl für Technische Chemie, Ruhr-Universität Bochum, D-44780 Bochum, Germany

Received: July 11, 2008; Revised Manuscript Received: August 25, 2008

Structural characteristics and catalytic activity of nanosized ceria−terbia mixed oxides have been investigated using X-ray diffraction (XRD), transmission electron microscopy (TEM), X-ray photoelectron spectroscopy (XPS), ion scattering spectroscopy, temperature-programmed reduction/oxidation, and Brunauer−Emmett−Teller surface area techniques. The catalytic usefulness has been evaluated for oxygen storage-release capacity (OSC) and CO oxidation activity. The XRD and TEM results suggest that the crystallite sizes of these nano-oxides are in the range 5−12 nm within the investigated temperature range of 773−1073 K. The mixed oxide solid solutions adopted a fluorite-type structure and exhibited cell parameters with respect to Vegard's rule. The XPS measurements revealed that both cerium and terbium are in 3+ and 4+ oxidation states, 4+ being dominant in both cases. The reduction temperature of the Ce−Tb oxide is observed to be lower than that of the pure ceria and exhibited better redox properties due to the formation of solid solution. The OSC is substantially higher for the mixed oxide, and the presence of oxygen vacancies favored better CO oxidation activity. The nanosized ceria−terbia mixed oxide is also found to be thermally quite stable and capable of manifesting redox behavior after severe heat treatment.

Introduction

There has been a sustained interest in the development of new catalysts having additional advantages to the environmental issues.[1−7] Air pollution is one of the major global problems in recent times. Three-way catalysts (TWC) for automotive exhaust treatment, which transform three environmentally hazardous gases, namely, CO, NO_x, and hydrocarbons to environmentally benign or less hazardous form, is therefore a topic of intensive research. Ceria (CeO_2) is an important ingredient in the formulation of TWCs.[1−4] The ability of ceria to release oxygen by forming oxygen vacancies under oxygen-poor (reducing) conditions and, conversely, to store oxygen by filling oxygen vacancies under oxygen-rich (oxidizing) conditions is utilized to stabilize the air-to-fuel ratio at the desired level.[4] Obviously, the oxygen storage/release capacity (OSC) of ceria plays a vital role in this regard. Besides, many technological and bioapplications have also been benefited from the unique redox and transport properties of ceria and ceria-based materials.[6−12]

Ceria-based mixed oxides exhibit improved OSC and lower reduction temperatures than pure ceria.[13−17] Dissolution of different 4+ cations in the ceria structure influences the oxygen diffusivity within the lattice. It influences how fast the bulk ceria material can exchange oxygen with the surrounding environment.[18] The defect generation in the ceria lattice also determines the ease of this possibility. When a vacancy is formed, the transformation from Ce^{4+} into Ce^{3+} takes place. Therefore, this process is influenced by the presence of 4+ solute ions. The Ce^{3+} ions (ionic radii 1.14 Å) are larger than the Ce^{4+} ions (0.97 Å), and the formation of Ce^{3+} vacancy clusters distorts the surrounding fluorite lattice. By formation of solid solutions with 4+ ions of smaller size than Ce^{4+} itself, e.g., Hf^{4+}, Zr^{4+}, Tb^{4+}, etc., the energetic cost of these distortions can be decreased.[19] The diffusivity is governed by the activation energy of diffusion, which is identified as the sum of the migration barrier for moving an oxygen ion from one lattice site to a neighboring vacant site and the binding energy between vacancies and tetravalent solutes.[19] In this context, it is important to understand how different 4+ ions influence the redox properties of ceria. To date, ceria−zirconia composite oxides have been most extensively studied.[4,20,21] Recently, we have demonstrated the influence of Hf^{4+} doping on the catalytic performance of ceria-based nano-oxides.[20] The use of variable valence dopants has also attracted lot of interest.[4,8,22−30] The primary aim of these studies has been to improve the OSC property. The stability at high temperatures and better chemical reactivity by introducing O vacancies in the ceria lattice are the other goals. However, these systems are highly complicated, and accordingly the structural information is relatively scarce.[4,6] Moreover, despite a number of investigations probing into the oxygen storage/release property of ceria-based materials, there are important issues that remain unclear. The excellent OSC is an inherent property of ceria in the cubic fluorite structure.[31] On the microscopic level, the removal of an oxygen atom is made possible due to the ability of the cerium atom to easily and drastically adjust its electronic configuration to best fit its immediate environment.[31,32] Though the ceria−zirconia mixed oxides are better oxygen storage materials than pure ceria, the role of zirconia is still ambiguous, whether it is a mere size

* To whom correspondence should be addressed. E-mail: mreddyb@yahoo.com.
† Indian Institute of Chemical Technology.
‡ National Institute of Advanced Industrial Science and Technology.
§ Ruhr-Universität Bochum.

10.1021/jp806131r CCC: $40.75
Published on Web 09/27/2008

effect or anything else.[33] Some reports could be found in the literature where special emphasis is given on the size effect of different dopant ions.[19,34]

By consideration of the success of ceria-based materials and their importance in today's TWC formulations, the overall outlook is that ceria-containing materials will remain as major components of automotive exhaust catalysts in the long run. Special uses of oxygen storage materials will likely emerge in response to lower emission standards and increased fuel economy requirements. Motivated by these facts research continues into new oxygen storage materials aimed at specific applications. As a lanthanide, it is interesting to investigate the effect of Tb when doped into the ceria lattice, another lanthanide oxide.[8,18,22−29] Again, Tb exhibits variable valence states (3+ and 4+), which may have some impact on the final product. The present study has been undertaken against the aforesaid background and devoted to the structural analysis of the ceria−terbia composite oxides obtained by a coprecipitation method. The structural evolution has been investigated using X-ray diffraction (XRD), transmission electron microscopy (TEM), X-ray photoelectron spectroscopy (XPS), ion-scattering spectroscopy (ISS), temperature-programmed reduction/oxidation (TPR-TPO), and Brunauer−Emmett−Teller (BET) surface area techniques. The catalytic performance was evaluated for OSC and CO oxidation activity.

Experimental Procedures

Ceria−terbia (CT, 80:20 mol % based on oxides) solid solution was prepared by adopting a coprecipitation method using ammonium cerium(IV) nitrate (Loba Chemie, GR grade) and terbium(III) nitrate (Aldrich, AR grade) respectively. The desired amounts of precursors were dissolved separately in double-distilled water under mild stirring conditions and mixed together. Upon complete mixing, excess ammonium hydroxide was added dropwise until the precipitation was complete (pH = ∼8.5). The resulting slurry was filtered off and thoroughly washed with distilled water until free from anion impurities. The accumulated mixed oxide paste was carefully placed and covered in a clean ceramic crucible and allowed to dry overnight in a hood. It was then oven dried at 393 K for 12 h. Finally, it was divided into four parts and calcined at 773, 873, 973, and 1073 K, respectively, for 6 h in air atmosphere to remove water and any residual precursors remaining from the coprecipitation step. After cooling, the solid residues were ground using a ceramic mortar and pestle until fine powders were obtained.

Powder XRD patterns were recorded on a Rigaku Multiflex instrument using nickel-filtered Cu Kα (0.15418 nm) radiation source and a scintillation counter detector. The intensity data were collected over a 2θ range of 2−80° with a 0.02° step size and using a counting time of 1 s per point. The XRD phases present in the samples were identified with the help of Powder Diffraction File-International Center for Diffraction Data (PDF-ICDD). The average crystallite size of oxide phases was estimated with the help of Debye−Scherrer equation using the XRD data of all prominent lines and the lattice parameter was calculated by a standard cubic indexation method using the intensity of the most prominent peak (111).

The BET surface areas were determined by N_2 adsorption−desorption at liquid N_2 temperature, on a Micromeritics Gemini 2360 instrument. Prior to analysis, the samples were oven-dried at 393 K for 12 h and flushed with Argon gas for 2 h.

The XPS measurements were made on a Shimadzu (ESCA 3400) spectrometer by using Mg Kα (1253.6 eV) radiation as the excitation source. Charging of catalyst samples was corrected by setting the binding energy (BE) of the adventitious carbon (C 1s) peak at 284.6 eV.[35] The finely ground oven-dried samples were placed on a double-stick graphite sheet and mounted on the standard sample holder. The sample holder was transferred to the analysis chamber through a rod attached to it. The XPS analysis was done at room temperature, and pressures were typically on the order of less than 10^{-8} Pa. The samples were outgassed in a vacuum oven overnight before XPS measurements. The TEM studies were made on a JEM-2010 (JEOL) instrument equipped with a slow-scan CCD camera and at an accelerating voltage of 200 kV. Samples were sonically dispersed in ethanol and deposited on a carbon-coated copper grid before examination.

IS spectra were measured in a Leybold surface analysis system equipped with X-ray and ion sources and an EA 10/100 electron (ion) analyzer with multichannel detection (Specs). Samples were pretreated in flowing synthetic air (20% O_2/N_2) at 573 K for 30 min before they were introduced into the spectrometer vacuum without further contact with the ambient humid atmosphere (in situ treatment). The measurements were done with 3000-eV Ar+ ions and recorded with the analyzer in pass-energy mode (pass energy 84.5 eV). The surface charge was removed with a flood gun. The source and the flood gun were allowed to stabilize with the sample withdrawn from the measurement position. Signal intensities were estimated assuming the background to be linear.

The redox property of the 773 K calcined CT sample has been studied by TPR-TPO experiments. The measurement system is equipped with a thermal conductivity detector. Before starting TPR runs, the sample was activated under flowing O_2 (9.35%)/Ar at 573 K for 30 min maintaining the heating rate of 10 K/min. The sample was then cooled to 273 K. TPR was performed by heating the sample at 5 K/min up to 1073 K in a H_2 (4.2%)/Ar flow (84.1 mL/min). The sample was held at 1073 K for 1 h. The TPO experiment was performed following TPR after the sample was cooled in H_2 (4.2%)/Ar flow to 273 K. After that the sample was heated to 1073 K at a rate of 10 K/min under a flow of O_2 (5%)/Ar (100 mL/min). Then the reoxidized sample was cooled in the same environment to 273 K, and the second reduction run (TPR-2) was carried out followed by second oxidation run (TPO-2) under the same reaction conditions as the first TPR-TPO runs.

The OSC was determined by the oxygen release characteristics of the sample in the temperature region 573−1073 K with the help of thermogravimetric method. The change in the weight of the sample was monitored by thermogravimetry (TG) under cyclic heat treatments in flowing nitrogen or dry air. A commercial Netzsch TG-DTA analyzer (Luxx, STA, 409 PC, Germany) was employed for this purpose. The heat cycle consisted of heating the sample to 1073 K, cooling to 423 K, and again heating to 1073 K. All heating and cooling rates were 5 K/min. The weight loss of the sample during the second heating cycle was used to measure the oxygen release properties. This method is essentially similar to the one reported by Ozawa et al.[15]

The catalytic activity of the synthesized nanocomposite oxides was evaluated for the oxidation of CO at normal atmospheric pressure and temperatures in the range of 300−773 K in a fixed bed microreactor at a heating ramp of 5 K/min. About 100 mg catalyst sample (250−355 μm sieve fraction) diluted with quartz particles of the same sieve fraction was placed in a quartz reactor for evaluation. Temperature was measured directly at the catalyst bed, using a thermocouple placed in the hollow part of the reactor. The following gases and gas mixtures were used

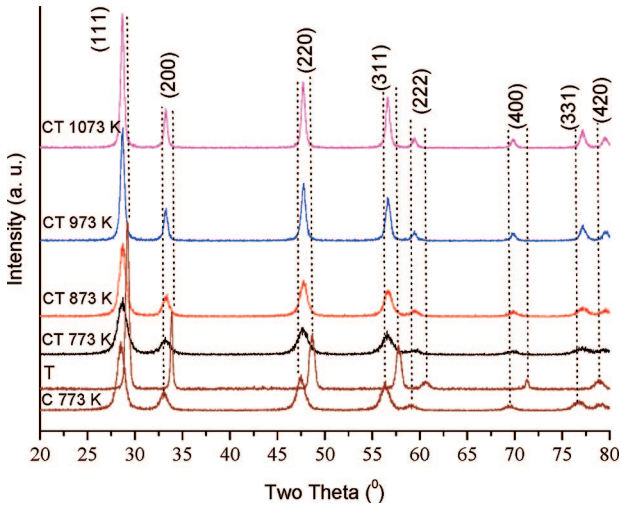

Figure 1. Powder XRD patterns of ceria−terbia samples calcined at various temperatures along with 773 K calcined CeO_2 (C, 773 K) and terbium oxide (T).

(supplied by Air Liquide): argon (>99.999% purity), 9.98% CO in argon (CO purity, >99.997%; argon purity, >99.99%), and 10.2% O_2 in argon (oxygen purity, >99.995%). The total flow rates maintained by three mass flow controllers were in the range of 50−60 N mL/min (milliliters normalized to 273.15 K and 1 atm.). The CO and CO_2 gas concentrations were measured using an Uras 14 infrared analyzer module, and the O_2 concentration was measured using a Magnos 16 analyzer (Hartmann & Braun). Prior to oxidation of CO, the catalysts were heated to 773 K in 10.2% O_2/Ar gas mixture, using a heating ramp of 10 K/min, and kept at the final temperature for 1 h. The oxidized sample was then purged in argon and cooled to the desired starting temperature. The CO/O_2 reactant feed ratio was 1, and partial pressures of CO and O_2 were in the range of 10 mbar.

Results and Discussion

Powder XRD patterns of Ce−Tb oxides calcined at different temperatures along with pure cerium and terbium oxides calcined at 773 K are shown in Figure 1. The XRD profiles of the mixed oxide samples clearly indicate the solid solution formation and correspond to the fluorite-type lattice. In particular, no XRD lines pertaining to terbium oxide were observed. The broadened lines indicate the presence of smaller particles of nanometer size. It is to be noted that a demixing of the mixed oxide phases with different cation ratios and cell parameters, as occurs for Ce−Zr oxides upon high temperature treatment,[36] has not been observed in the present study. Although single-phase patterns are observed for the Ce−Tb oxides, it must be noted that the relatively large peak widths obtained for the nanosized materials disallows to extract a consensus whether small amounts of segregated phases or concentration gradients within the mixed oxide materials could be present at a more or less local level. The Ce−Tb oxide samples reveal high BET surface area: 85 $m^2\ g^{-1}$ for 773 K calcined sample and gradually decreased to 37 $m^2\ g^{-1}$ after calcination at 1073 K (Table 1). Gradual sharpening of the XRD peaks with increasing calcination temperature could be observed as a result of sintering. This indicates an improvement in the crystallinity with corresponding increase in crystallite size and decrease in specific surface area after calcination at 873−1073 K. The calculated *a* cell parameter values for the mixed oxide samples reveals incorporation of terbium cation into the ceria lattice having smaller cell dimension than ceria (unit cell constant $a = 5.410$ Å), varying negligibly with temperature (Table 1). Tb^{3+} has an ionic radius similar to that of Ce^{4+},[37] whereas that of Tb^{4+} is much lower ($a = 5.213$ Å in TbO_2, i.e., by 3.7% lower than in CeO_2;[38] the ionic radii values for Ce^{4+}, Tb^{4+}, Ce^{3+}, and Tb^{3+} are 0.97, 0.88, 1.14, and 1.04 Å, respectively).[39] By assumption that the Vegard's rule is obeyed by the mixed oxides, the lattice parameters obtained for the Ce−Tb oxides are larger than expected if the whole terbium is present as Tb^{4+}. Hence, a part of terbium must be present as Tb^{3+} leading to a proportional amount of intrinsic oxygen vacancies for fulfilling electroneutrality requisites.[39] In case of 1073 K calcined sample, the cell parameter value is comparatively small. So there is a possibility that the amount of Tb^{4+} is slightly high in this sample. There is also a possibility that all terbia may not be fully incorporated in the process of mixed oxide formation. However, XRD results reveal no presence of terbia in crystalline form. But we cannot rule out the possibility of the presence of terbia in amorphous state. Further explanation is provided in the later part of our discussion.

TABLE 1: BET Surface Area, Average Crystallite Size, *a* Cell Parameter, and OSC of Ceria−Terbia Mixed Oxide Calcined at Different Temperatures

sample	BET SA (m^2g^{-1})	crystallite size (nm)[a]	lattice parameter (Å)[a]	OSC in terms of μmoles O_2/g ceria
CT 773	85	5.5	5.37	217.14
CT 873	67	6.2	5.37	
CT 973	52	8.3	5.37	
CT 1073	37	12.1	5.36	

[a] From XRD analysis.

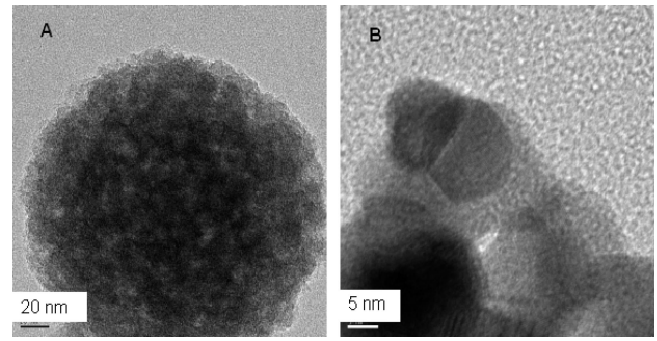

Figure 2. TEM (A) and HREM (B) micrographs of 773 K calcined ceria−terbia sample.

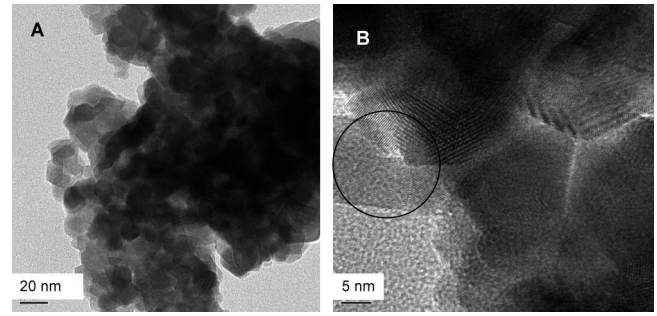

Figure 3. TEM (A) and HREM (B) micrographs of 1073 K calcined ceria−terbia sample.

The nanometric sizes of the particles are confirmed by TEM−HREM analysis. The representative micrographs of 773 and 1073 K calcined samples are presented in Figures 2 and 3, respectively. The obtained micrographs reveal agglomerated microstructures. However, plain faces of crystallites could not be seen in Figure 2, which suggest that a large part of the

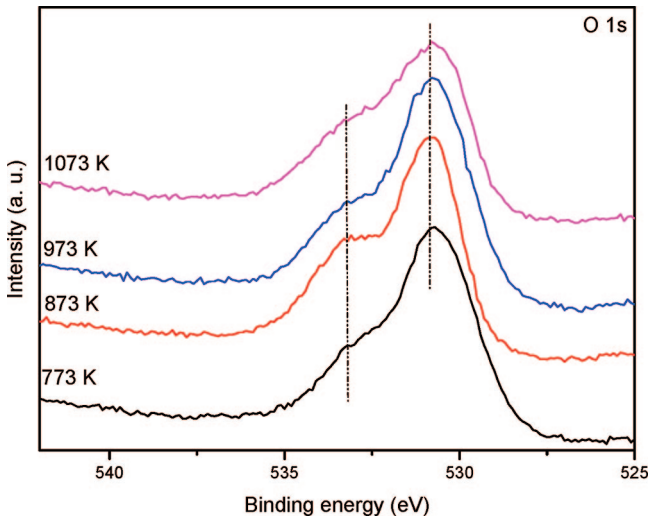

Figure 4. O 1s XPS patterns of ceria−terbia samples calcined at various temperatures.

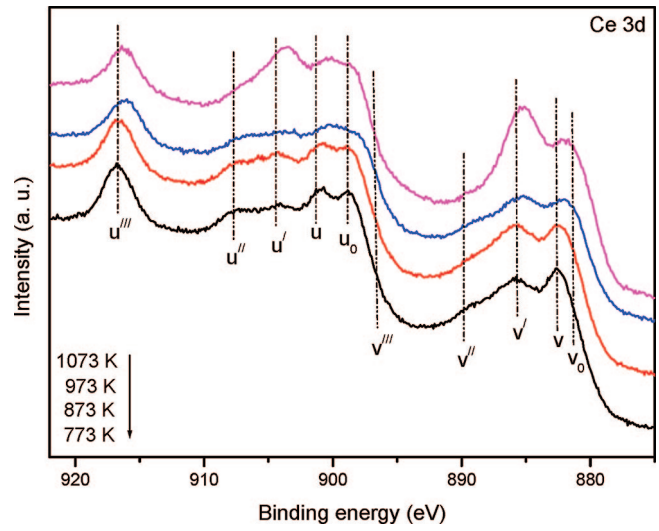

Figure 5. Ce 3d XPS patterns of ceria−terbia samples calcined at various temperatures.

material is still amorphous. It is observed from Figure 2 that the particles have the dimension of ∼5−6 nm. The mixed oxide samples show an increase in particle size with temperature increase. As revealed by Figure 3, the particle sizes increase to ∼12 nm after calcination at 1073 K. The shapes of the particles observed were almost similar to those usually seen in previous works for ceria or ceria−zirconia specimens.[40] The cuboctahedral shapes were clearly dominant in both the cases. Interestingly, in case of 1073 K calcined sample (Figure 3B), very few near-rectangular shapes could also be seen (encircled area). This may be due to the occurrence of (100) plane terminations. It is known that for CeO_2 the most stable exposed surfaces are (111) and (110),[41] while the (100) surface needs a substantial number of anion vacancies to be stabilized. It may be possible that the number of vacancies present during the high temperature treatment allow such surfaces to stabilize leading to the observed particle shapes. This should be taken into account when surface reactivity of these materials is analyzed, which may become modified to some extent if the crystal plane that is preferentially exposed changes. However, from XRD analysis, no information regarding the stabilization of the (100) surface in case of 1073 K calcined sample could be obtained. The HREM images (Figures 2B and 3B) show some overlapping regions of the mixed oxide particles, which may be responsible for better catalytic activity.

The O 1s core level XPS profiles of Ce−Tb oxide samples calcined at different temperatures are presented in Figure 4. It is obvious from the figure that the patterns are dominated by a broad peak at 530.8 eV attributed to the lattice oxygen associated with the Ce−Tb oxides and another at a slightly higher binding energy side featuring absorbed oxygen species (presumably from absorbed water and/or carbonates).[35,42] XPS was primarily used to investigate the oxidation state of Ce in the mixed oxides. It is always challenging to use XPS to study ceria and ceria-based materials due to severe charging effect and comparatively larger charging corrections are needed in the BE values.[39] As known, the Ce 3d core level peak of ceria is complicated by the hybridization of the O 2p valence band with Ce 4f level, which results in several final states for cerium.[43,44] Also the spectra consist of a number of overlapping peaks making it difficult to get unique and consistent results.[39] Figure 5 shows the Ce 3d spectra of the mixed oxide samples calcined at different temperatures. Two sets of spin−orbit multiplets featuring $3d_{3/2}$ and $3d_{5/2}$ are represented as u and v, respectively. Here, the

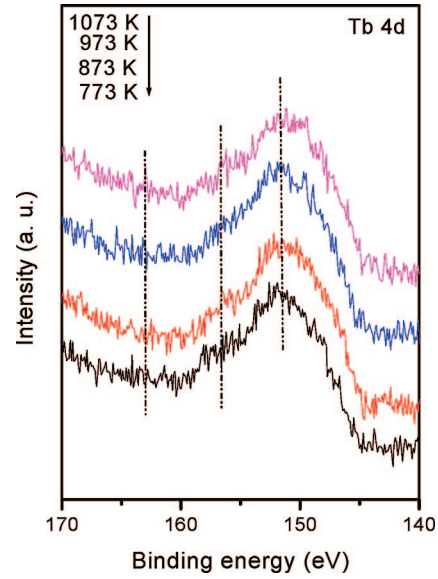

Figure 6. Tb 4d XPS patterns of ceria−terbia samples calcined at various temperatures.

peaks at ∼882.0 eV (v) and 901.1 eV (u) are the main lines of Ce^{4+}, whereas features at 889.6 eV (v''), 897.8 eV (v'''), 907.5 eV (u''), and 916.6 eV (u''') are satellites related to the Ce^{4+} state. The main signals of Ce^{3+} (v_0 and u_0) would be expected below 881 eV and around 898 eV, the latter overlapping with v'''. The satellites to these features (v' and u') occur at 885.5 and 904.2 eV, respectively. The absence of a peak at 881 eV reveals that Ce is predominantly in the 4+ oxidation state, which is confirmed by the considerable intensity of the u''' component, which has no parallel in the Ce^{3+} satellite structure. However, significant intensity is also seen around 885 eV indicating the presence of Ce^{3+} in the sample (the main Ce^{3+} v_0 component causes just a widening of the 882-eV feature assigned to v). Thus, the surface of the present samples contains Ce both in the 4+ and the 3+ states. At higher calcination temperatures, the increased intensity at 885 eV (v') and decreased intensity at 916 eV (u''') suggest a lower average oxidation degree of the surface Ce ions. Figure 6 shows the Tb 4d spectra of the mixed oxide samples. For terbium, Tb 3d core level analysis using a conventional laboratory spectrometer (with either Mg or Al Kα radiation) is very difficult as photoemitted electrons are of very

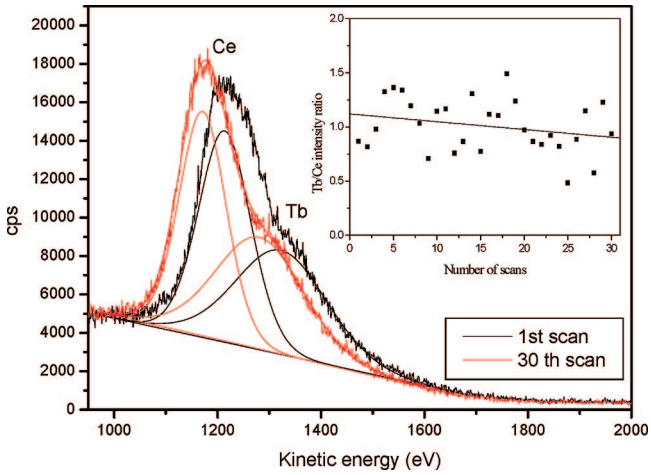

Figure 7. ISS pattern of ceria−terbia sample calcined at 773 K after first and 30th scan. Inset: plot of Tb/Ce intensity ratio.

low kinetic energies. Therefore, next most intense core level (Tb 4d) is used for analysis. Not much literature is available about the assignment of Tb oxidation states in Tb 4d spectra,[45−47]but there is agreement that Tb^{3+} gives a signal below 150 eV, whereas Tb^{4+} is related to features well above 150 eV (according to ref 47 at 155 eV). The spin−orbit splitting of Tb (4d) is too small to be resolved by a laboratory instrument; therefore, a single asymmetric line would be expected if a single oxidation state was present. The spectra obtained, with their pronounced shoulder below 150 eV, a maximum at 151.7 eV and a tailing toward 160 eV shows instead the presence of more than one oxidation state, i.e., the surface of our Ce−Tb mixed oxide contains the Tb both in the 3+ and the 4+ oxidation state. On the basis of the expectation of Tb^{4+} at 155 eV,[47] one may conclude that the contributions of both valence states are comparable because the maximum of the experimental signal is well in between the BE values of the pure 3+ and 4+ states. With increasing calcination temperature the intensity of the low-energy shoulder seems to decrease slightly, suggesting a somewhat higher Tb^{4+} contribution after severe calcinations, but the considerable noise level on the spectra obtained prevents a clear-cut conclusion on this point.

The Ar-ISS spectra of 773 K calcined Ce−Tb oxide sample after definite scans (1st and 30th scans) are presented in Figure 7. It is obvious from the figure that there is a shoulder at the Ce peak, which can be assigned to Tb. The assignment is based on the kinetic energy difference between the second signal and the Ce peak, although this difference cannot be determined very accurately due to incomplete separation of the features. This result shows that Tb is really exposed on the surface of the mixed oxides. The signals have been fitted by two components as shown in the figure. The Tb surface concentration is, however, not accessible as sensitivity factors are not available. Upon extended sputtering of the surface, the signal shape remains unchanged, and no trend can be discerned in the Tb/Ce intensity ratio. A small shift in the position of the Ce and Tb peaks after the sputter series is probably a detector artifact as a result of instability in the system. It is clear from Figure 7 that the composition of the mixed oxide does not change below the surface.

The investigation of reduction/oxidation properties was performed for the 773 K calcined Ce−Tb oxide sample using a TPR-TPO method, and the results are shown in Figure 8. For this sample, the reduction can happen for the Ce^{3+}/Ce^{4+} couple and/or the Tb^{3+}/Tb^{4+} couple. Generally, the H_2-TPR of ceria gives two peaks at around 753 and 1168 K attributed to the successive reduction of the surface and the bulk ceria.[48,49] In the case of ceria−zirconia mixed oxides, however, only one broad peak is observed and many researchers suggest that surface and bulk reduction cannot be distinguished by the conventional TPR technique since both processes occur almost simultaneously during TPR measurement.[50,51] Interestingly, in the present case, two regions of reduction are distinctly observed. Although similar to that of CeO_2 alone, for Ce−Tb oxide which has a ceria content of more than 50 mol %, the peak at the low temperature region became very prominent. Obviously, such a peak could not be ascribed only to the reduction of the surface oxygen because of the dominant H_2 consumption of the low-temperature peaks.[52] During first TPR run (Figure 8a), the initial reduction is taking place ranging from 473 to 873 K. Interestingly, the peak splits into a triplet. Literature reveals that TPR profile of $TbO_{1.75}$ shows reduction bands at 576, 940, and 993 K.[45] Therefore, the splitting of the first reduction region is presumably due to the $Tb^{4+} \rightarrow Tb^{3+}$ reduction along with Ce^{4+} reduction and broad particle size distribution. Obviously, the addition of Tb to CeO_2 resulted in shifting the reduction peak to a lower temperature. The second reduction peak starts at around 873 K having maxima at below 1073 K, which was reported to be due to the reduction of the bulk oxides.[48,53] The reduction of the bulk lattice oxygen in the solid solution becomes easier because of the distortion of the structure, which is caused by the partial substitution of Ce^{4+} with Tb^{4+}. This occurs through structural modifications of the fluorite-type lattice of ceria as a consequence of the substitution of Ce^{4+} (ionic radius 0.97 Å) with Tb^{4+} (ionic radius 0.88 Å). The effect of this substitution is to decrease cell volume, lowering the activation energy for oxygen-ion diffusion within the lattice, and consequently favoring reduction.[52] The TPO experiment (TPO-1, Figure 8b) shows that the complete reoxidation of the reduced sample was possible at around 363 K as no additional O_2 was adsorbed by the mixed oxide at higher temperatures (up to 1073 K). The TPR-2 (Figure 8c) profile indicates that the sample is highly reducible at that stage also. However, the reduction behavior is somewhat changed in this run. Two distinct peaks, attributed to surface and bulk reduction of ceria, are observed at higher temperatures compared to the first run. This is obvious because the particle size is increased after exposing the sample up to 1073 K. Interestingly, the TPO-2 profile as shown in Figure 8d is completely similar to that obtained for TPO-1 run. Thus the TPR-1/TPO-1/TPR-2/TPO-2 cycle revealed that the sample is thermally quite stable and capable of manifesting redox behavior after severe heat treatment.

The formation of reduced oxides is a combined process of formation, migration, and ordering of Ce^{3+} vacancy complexes. When the external conditions change from oxygen poor to oxygen rich, this process behaves reversibly. This makes the oxygen storage-and-release ability of ceria a remarkable property used in many modern environmentally friendly applications.[31] The OSC of Ce−Tb oxide sample calcined at 773 K was found to be 217.14 μmoles O_2/g ceria [170 μmoles O_2/g Ce−Tb oxide corresponding to 0.55% weight loss as described in the experimental section; in terms of oxygen vacancy concentration (δ), it corresponds to a value of 0.18], which is almost four times that obtained for pure ceria sample.[4] This implies significant enhancement in OSC after incorporation of terbia into the ceria lattice. It is known that fluorite-type structure plays an important role for the OSC.[4] The presently investigated system shows the same structure as revealed by XRD analysis, and therefore this enhancement in OSC is expected. The

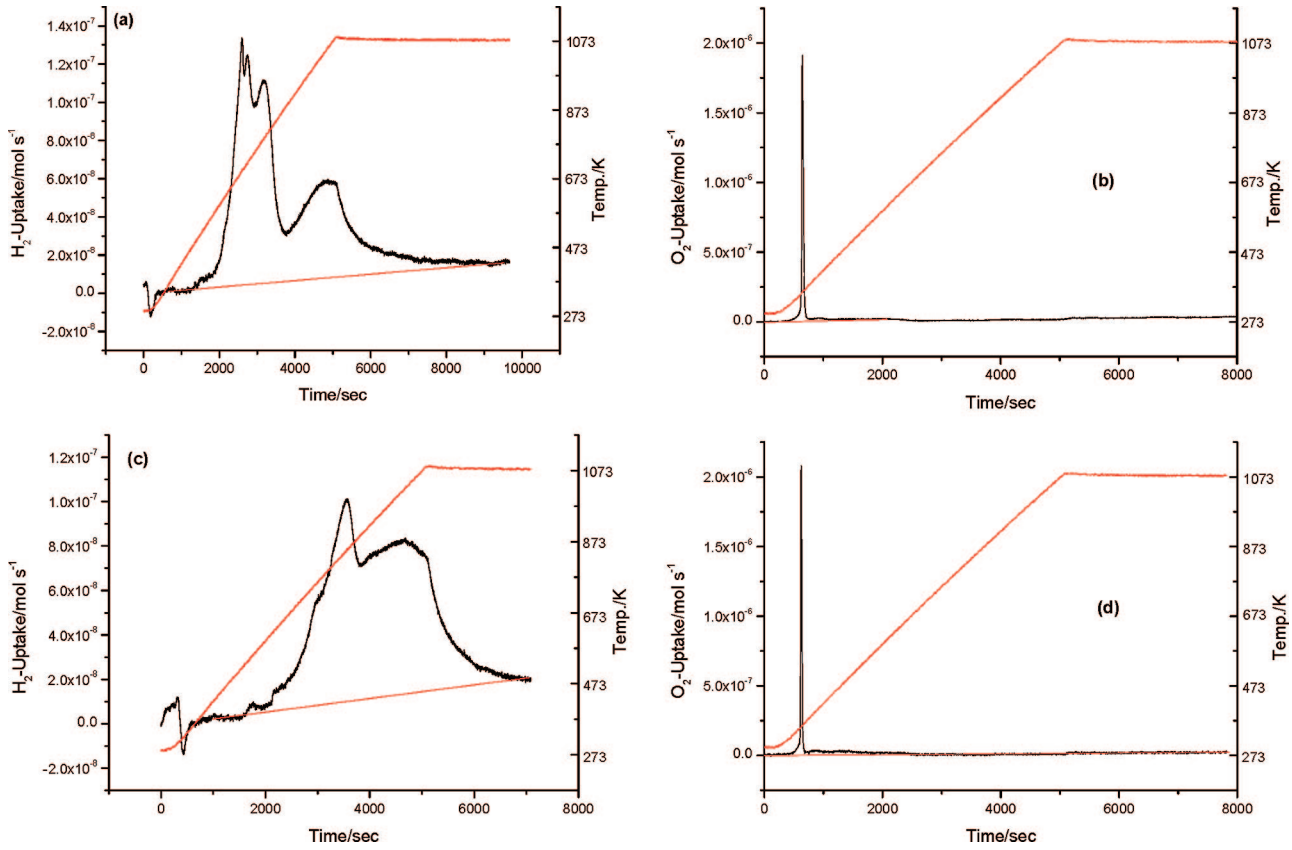

Figure 8. TPR-TPO patterns of 773 K calcined ceria−terbia (CT) sample (a) first TPR run, (b) first TPO run, (c) second TPR run, and (d) second TPO run.

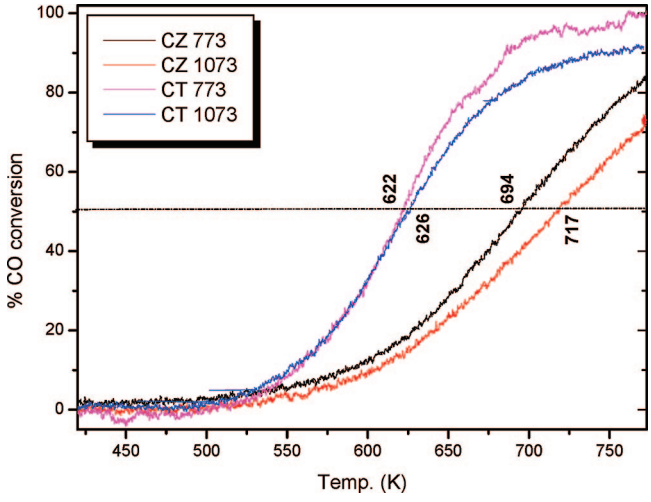

Figure 9. Conversion of CO over ceria−zirconia (CZ) and ceria−terbia (CT) samples calcined at 773 and 1073 K as a function of reaction temperature.

specificity of mixed oxides for oxygen storage was shown to be due to the participation of bulk oxygen.[54] Hence, another important point, which can be drawn from the obtained results, is that the oxygen storage takes place not only at the surface but also in the bulk. Also like the ceria−zirconia system, the introduction of Tb induces the formation of structural defects associated with oxygen vacancies inline with earlier reports.[55]

The catalytic activity for CO oxidation of the Ce−Tb oxide samples calcined at 773 and 1073 K in the temperature range 400 to 773 K are represented in Figure 9. For comparison purposes, the results obtained for the respective Ce−Zr oxide (1:1 mol ratio) samples are also included in the figure. It is well-known that Ce−Zr oxide is superior to pure ceria in terms of its stability and catalytic activity. Therefore, we preferred to compare with the Ce−Zr oxide sample. The details of its preparation and physicochemical characteristics could be found in our earlier reports.[20,40] It is evident from Figure 9 that the Ce−Tb oxide samples are exhibiting better activity in terms of total conversion as well as light off temperature (50% conversion). The Ce−Tb oxide sample calcined at 773 K shows ∼100% conversion at 773 K (highest temperature investigated), and after calcination at 1073 K also exhibits more than 90% conversion. The nominal decrease in the activity may be due to the loss of surface area after exposing the sample to 1073 K. On the other hand, Ce−Zr oxide provides 85 and 70% conversion (for 773 and 1073 K calcined samples, respectively) under the same experimental conditions. Another interesting observation is that the light-off temperature for Ce−Tb oxide samples does not vary significantly. This observation is inline with the results obtained from TPR-TPO experiments. Thus, better thermal stability and redox property thereby leading to remarkable OSC and CO oxidation activity make Ce−Tb oxide very promising and another alternative catalyst in the modern TWC catalyst formulations.

Conclusions

Doping of a variable valence element, namely, terbium, into the ceria lattice has shown that solid solution formation is taking place and that the mixed oxide is highly thermo-stable. These conclusions are backed by XRD analysis as the position of XRD peaks for mixed oxides differ slightly from both ceria and terbia alone, and no phase segregation is evident up to 1073 K calcination temperature. The cell *a* parameter values hint the possibility of the presence of Tb in both 3+ and 4+ oxidation

states. The crystallite size of the prepared samples falls in the nanometer range as evident from XRD and TEM-HREM analysis. The TEM-HREM micrographs also clearly revealed fluorite structure of the mixed oxides, which did not change even after high temperature calcination treatment. The XPS analysis indicated that Ce and Tb were present in both 3+ and 4+ oxidation states, and the latter is dominant. ISS analysis showed that the Tb/Ce intensity ratio in the sputter series maintained a parallel trend revealing no surface enrichment of cerium. The TPR-TPO measurements suggested that the addition of Tb to CeO_2 resulted in shifting of the reduction peaks (surface and bulk reductions) to lower temperatures. This also indicates the distortion of the ceria structure, which is possible by the partial substitution of Ce^{4+} with Tb^{4+}. From the results of the TPR-TPO cycles, it can be concluded that the sample is thermally quite stable, and after severe heat treatment also its redox behavior remains intact. Significant enhancement in the OSC value after incorporation of Tb into the ceria lattice was found which is almost four times in comparison to pure ceria. In terms of conversion as well as light-off temperature (50% conversion), the ceria−terbia composite oxides are remarkably better catalysts. These samples calcined at 773 and 1073 K gave more than 90% CO conversion at 773 K (highest temperature investigated), and the difference in light off temperature was very minimal (only 4 K). Thus, ceria−terbia mixed oxide could be a promising catalyst for use in TWC formulations.

Acknowledgment. We thank Dr. Tetsuo Umegaki, AIST-Kansai, Japan, Dr. Sergij Merzlikin and Ms. S. Buse, RUB, Germany for help in XPS, ISS, and TPR-TPO measurements, respectively. P.S. and P.B. thank Council of Scientific and Industrial Research (CSIR), New Delhi, for research fellowships. Thanks are due to DST, New Delhi, and DAAD, Germany, for financial support under a bilateral collaboration program (DST-DAAD-PPP-2005).

References and Notes

(1) Fu, Q.; Saltsburg, H.; Stephanopoulos, M. F. *Science* **2003**, *301*, 935.
(2) Steele, B. C. H.; Heinzel, A. *Nature* **2001**, *414*, 345.
(3) Garcia, M. F.; Arias, A. M.; Hanson, J. C.; Rodriguez, J. A. *Chem. Rev.* **2004**, *104*, 4063.
(4) Trovarelli, A. In *Catalysis by Ceria and Related Materials, Catalytic Science Series*; Hutchings, G. J., Ed.; Imperial College Press: London, 2002; Vol. 2.
(5) Arias, A. M.; Hungria, A. B.; Garcia, M. F.; Conesa, J. C.; Munuera, G. *J. Power Sources* **2005**, *151*, 32.
(6) Machida, M.; Murata, Y.; Kishikawa, K.; Zhang, D.; Ikeue, K. *Chem. Mater.* **2008**, *20*, 4489.
(7) Reddy, B. M.; Bharali, P.; Saikia, P.; Park, S.-E.; van den Berg, M. W. E.; Muhler, M.; Grünert, W. *J. Phys. Chem. C* **2008**, *112*, 11729.
(8) Wang, X.; Hanson, J. C.; Liu, G.; Rodriguez, J. A. *J. Chem. Phys.* **2004**, *121*, 5434.
(9) Vries, K. J. D.; Meng, G. Y. *Mater. Res. Bull.* **1998**, *33*, 357.
(10) Arias, A. M.; Hungria, A. B.; Garcia, M. F.; Juez, A. I.; Conesa, J. C.; Mather, G. C.; Munuera, G. *J. Power Sources* **2005**, *151*, 43.
(11) Chen, J.; Patil, S.; Seal, S.; McGinnis, J. F. *Nat. Nanotech.* **2006**, *1*, 142.
(12) Patil, S.; Reshetnikov, S.; Haldar, M. K.; Seal, S.; Mallik, S. *J. Phys. Chem. C* **2007**, *111*, 8437.
(13) Kaspar, J.; Fornasiero, P.; Graziani, M. *Catal. Today* **1999**, *50*, 285.
(14) Fornasiero, P.; Monte, R. D.; Rao, G. R.; Kaspar, J.; Meriani, S.; Trovarelli, A.; Graziani, M. *J. Catal.* **1995**, *151*, 168.
(15) Ozawa, M.; Matuda, K.; Suzuki, S. *J. Alloys Compd.* **2000**, *303−304*, 56.
(16) Boaro, M.; Trovarelli, A.; Hwang, J. H.; Mason, T. O. *Solid State Ionics* **2002**, *147*, 85.
(17) Rodriguez, J. A.; Hanson, J. C.; Kim, J. Y.; Liu, G.; Juez, A. I.; Garcia, M. F. *J. Phys. Chem. B* **2003**, *107*, 3535.
(18) Bernal, S.; Blanco, G.; Cauqui, M. A.; Corchado, P.; Pintado, J. M.; Izquierdo, J. M. R. *Chem. Commun.* **1997**, 1545.
(19) Andersson, D. A.; Simak, S. I.; Skorodumova, N. V.; Abrikosov, I. A.; Johansson, B. *Appl. Phys. Lett.* **2007**, *90*, 031909.
(20) Reddy, B. M.; Bharali, P.; Saikia, P.; Khan, A.; Loridant, S.; Muhler, M.; Grünert, W. *J. Phys. Chem. C* **2007**, *111*, 1878.
(21) Reddy, B. M.; Lakshmanan, P.; Bharali, P.; Saikia, P.; Thrimurthulu, G.; Muhler, M.; Grünert, W. *J. Phys. Chem. C* **2007**, *111*, 10478.
(22) Ye, F.; Mori, T.; Ou, D. R.; Zou, J.; Drennan, J. *Mater. Res. Bull.* **2007**, *42*, 943.
(23) Ye, F.; Mori, T.; Ou, D. R.; Takahashi, M.; Zou, J.; Drennan, J. *Renewable Energy* **2008**, *33*, 331.
(24) Galtayries, A.; Blanco, G.; Cifredo, G. A.; Finol, D.; Pintado, J. M.; Vidal, H.; Sporken, R.; Bernal, S. *Surf. Interface Anal.* **1999**, *27*, 941.
(25) Garcia, M. F.; Wang, X.; Belver, C.; Juez, A. I.; Hanson, J. C.; Rodriguez, J. A. *Chem. Mater.* **2005**, *17*, 4181.
(26) Bernal, S.; Blanco, G.; Cifredo, G. A.; Delgado, J. J.; Finol, D.; Gatica, J. M.; Izquierdo, J. M. R.; Vidal, H.; Hoser, A. *Chem. Mater.* **2002**, *14*, 844.
(27) Bernal, S.; Calvino, J. J.; Cifredo, G. A.; Finol, D.; Gatica, J. M.; Kiely, C. J.; Cartes, C. L.; Zheng, J. G.; Vidal, H. *Chem. Mater.* **2002**, *14*, 1405.
(28) Blanco, G.; Calvino, J. J.; Cauqui, M. A.; Corchado, P.; Cartes, C. L.; Colliex, C.; Omil, J. A. P.; Stephan, O. *Chem. Mater.* **1999**, *11*, 3610.
(29) Wang, X.; Hanson, J. C.; Rodriguez, J. A.; Belver, C.; Garcia, M. F. *J. Chem. Phys.* **2005**, *122*, 154711.
(30) Pu, Z. Y.; Lu, J. Q.; Luo, M. F.; Xie, Y. L. *J. Phys. Chem. C* **2007**, *111*, 18695.
(31) Skorodumova, N. V.; Simak, S. I.; Lundqvist, B. I.; Abrikosov, I. A.; Johansson, B. *Phys. Rev. Lett.* **2002**, *89*, 166601.
(32) Svane, A. *Phys. Rev. Lett.* **1994**, *72*, 1248.
(33) Baidya, T.; Hegde, M. S.; Gopalakrishnan, J. *J. Phys. Chem. B* **2007**, *111*, 5149.
(34) Balducci, G.; Islam, M. S.; Kaspar, J.; Fornasiero, P.; Graziani, M. *Chem. Mater.* **2000**, *12*, 677.
(35) Wagner, C. D.; Riggs, W. M.; Davis, L. E.; Moulder, J. F. In *Handbook of X-ray Photoelectron Spectroscopy*; Muilenberg, G. E., Ed.; Perkin-Elmer Corporation: Eden Prairie, MN, 1978.
(36) Jen, H. W.; Graham, G. W.; Chun, W.; McCabe, R. W.; Cuif, J. P.; Deutsch, S. E.; Tauret, O. *Catal. Today* **1999**, *50*, 309.
(37) Saiki, A.; Ishizawa, N.; Mizutani, N.; Kato, M. *J. Ceram. Soc. Jpn.* **1985**, *93*, 649.
(38) Gruen, D. M.; Koehler, W. C.; Katz, J. J. *J. Am. Chem. Soc.* **1951**, *73*, 1475.
(39) Hungria, A. B.; Arias, A. M.; Garcia, M. F.; Juez, A. I.; Ruiz, A. G.; Calvino, J. J.; Conesa, J. C.; Soria, J. *Chem. Mater.* **2003**, *15*, 4309.
(40) Reddy, B. M.; Khan, A. *Catal. Surv. Asia* **2005**, *9*, 155.
(41) Sayle, T. X. T.; Parker, S. C.; Catlow, C. R. A. *J. Chem. Soc. Chem. Commun.* **1992**, 977.
(42) Guodong, F.; Changgen, F.; Zhao, Z. *J. Rare Earths* **2007**, *25*, 42.
(43) Normand, F. L.; Fallah, J. E.; Hilaire, L.; Legare, P.; Kotani, A.; Parlebas, J. C. *Solid State Commun.* **1989**, *71*, 885.
(44) Mullins, D. R.; Overbury, S. H.; Huntley, D. R. *Surf. Sci.* **1997**, *409*, 307.
(45) Dai, H. X.; Ng, C. F.; Au, C. T. *J. Catal.* **2001**, *199*, 177.
(46) Blanco, G.; Pintado, J. M.; Bernal, S.; Cauqui, M. A.; Corchado, M. P.; Galtayries, A.; Ghijsen, J.; Sporken, R.; Eickhoff, T.; Drube, W. *Surf. Interface Anal.* **2002**, *34*, 120.
(47) Li, L.; Wei, Q.; Li, H.; Zhang, D.; Su, W. *Z. Phys. B* **1995**, *96*, 451.
(48) Yao, H. C.; Yao, Y. F. *Yu J. Catal.* **1984**, *86*, 254.
(49) Perrichon, V.; Laachir, A.; Bergeret, G.; Frety, R.; Tournayan, L.; Touret, O. *J. Chem. Soc. Faraday Trans.* **1994**, *90*, 773.
(50) Fally, F.; Perrichon, V.; Vidal, H.; Kaspar, J.; Blanco, G.; Pintado, J. M.; Bernal, S.; Colon, G.; Daturi, M.; Lavalley, J. C. *Catal. Today* **2000**, *59*, 373.
(51) Vidmar, P.; Kaspar, J.; Fornasiero, P.; Graziani, M. *J. Phys. Chem. B* **1998**, *102*, 557.
(52) Rumruangwong, M.; Wongkasemjit, S. *Appl. Organometal. Chem.* **2006**, *20*, 615.
(53) Johnson, M. F. L.; Mooi, J. *J. Catal.* **1987**, *103*, 502.
(54) Maider, Y.; Descorme, C.; Govic, A. M. Le; Duprez, D. *J. Phys. Chem. B* **1999**, *103*, 10999.
(55) Rossignol, S.; Especel, C. M.; Duprez, D. *Stud. Surf. Sci. Catal.* **2000**, *130D*, 3327.

JP806131R